ACS APPLIED MATERIALS & INTERFACES

Research Article

www.acsami.org

Copper Nanoparticles: Aqueous Phase Synthesis and Conductive Films Fabrication at Low Sintering Temperature

Dunying Deng, Yunxia Jin, Yuanrong Cheng, Tianke Qi, and Fei Xiao*

Department of Materials Science, Fudan University, 220 Handan Road, Shanghai 200433, P. R. China.

ABSTRACT: Conductive copper nanoinks can be used as a low-cost replacement for silver and gold nanoinks that are used in inkjet printing of conductive patterns. We describe a high-throughput, simple, and convenient method for the preparation of copper nanoparticles in aqueous solution at room temperature. Copper acetate is used as the precursor, hydrazine as the reducing agent, and short chain carboxylic acids as capping agents. The concentration of the carboxylic acid plays a key role in the preparation of such copper nanoparticles. Stable copper nanoparticles with a diameter of less than 10 nm and a narrow size distribution were prepared when high concentrations of lactic acid, citric acid, or alanine were used. Thermogravimetric analysis results showed that any lactic acid or glycolic acid adsorbed on the surface of the copper nanoparticles can be removed at a relatively low temperature, especially, glycolic acid, which can be removed from the surface at about 125 °C. Highly conductive copper films prepared using lactic acid and glycolic acid as capping agents were obtained by drop coating a copper nanoparticle paste onto a glass slide followed by low temperature sintering. The electrical resistivity of the copper film using glycolic acid as the capping agent was 25.5 ± 8.0 and 34.8 ± 9.0 $\mu\Omega$·cm after annealing at 150 and 200 °C for 60 min under nitrogen, respectively. When lactic acid was used as the capping agent, the electrical resistivity of the copper films was 21.0 ± 7.0 and 9.1 ± 2.0 $\mu\Omega$·cm after annealing at 150 and 200 °C for 60 min under nitrogen, respectively, with the latter being about five times greater than the resistivity of bulk copper (1.7 $\mu\Omega$·cm).

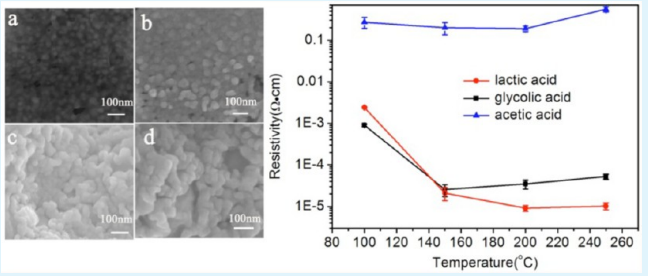

KEYWORDS: *copper nanoparticles, short chain carboxylic acids, sintering temperature, electrical resistivity, printed electronics*

1. INTRODUCTION

The unique properties of metallic nanoparticles offer the possibility of developing new products and have paved the way for new applications. The electronics industry has exploited the surface effects and small size effects of such particles for this purpose. Recently, considerable interest has been directed to developing conductive metal nanoinks for printable electronics on plastic substrates.[1−4] However, the surfaces of nanometer-sized metal particles are highly active making them liable to aggregate during synthesis unless their surfaces are coated with an organic protective layer. The small size effect of such metallic nanoparticles has been exploited to reduce the melting point and facilitate the sintering of such particles at low temperatures. For example, the melting temperature of gold nanoparticles of less than 5 nm in diameter is around 300 °C, whereas bulk gold melts at over 1000 °C.[5]

The basic requirements for the successful synthesis of metal nanoparticle inks include good dispersing stability and resistance to oxidation.[6,7] The ability to deposit a well dispersed silver nanoparticle ink on substrates using inkjet printing has been known for years.[8−10] However, the electrochemical migration of silver, often resulting in short circuit failure under high humidity conditions, and the high cost of this metal, limit the industrial application of silver-bearing inks.[11] Since copper is much cheaper than silver and possesses high conductivity, copper nanoparticles are suitable substitutes for silver nanoparticles. Copper nanoparticles for use in conductive inks have been primarily synthesized in organic solvent under an inert atmosphere using capping agents to prevent aggregation and oxidation of the nanoparticles.[12−16] However, most of the known synthesis methods are not economically feasible because of their low throughput. Furthermore, the reported capping agents (PVP, CTAB, oleic acids, alkanethiols, PPY, PEI, and TEPA),[16] which form a nonconductive shell around the surface of the copper nanoparticles, have a negative effect on the conductivity of the inkjet-printed pattern because of the high decomposition temperature of the capping agent. Conducting capping agents, such as polyaniline, exhibit not only limited conductivity compared with the metals, but are also insoluble in common organic solvents.[17] Inkjet-printed materials need to be processed at low temperatures to be used in combination with inexpensive plastic substrates which melt at low temperature. To reap the economic benefits of inkjet-printed electronics, economically feasible processes for the preparation of nanoparticles with low sintering temperature on a large scale are required.

Choi et al. have previously reported that the electrical resistivity of sintered copper nanoparticles (9 nm diameter)

Received: February 4, 2013
Accepted: April 11, 2013
Published: April 11, 2013

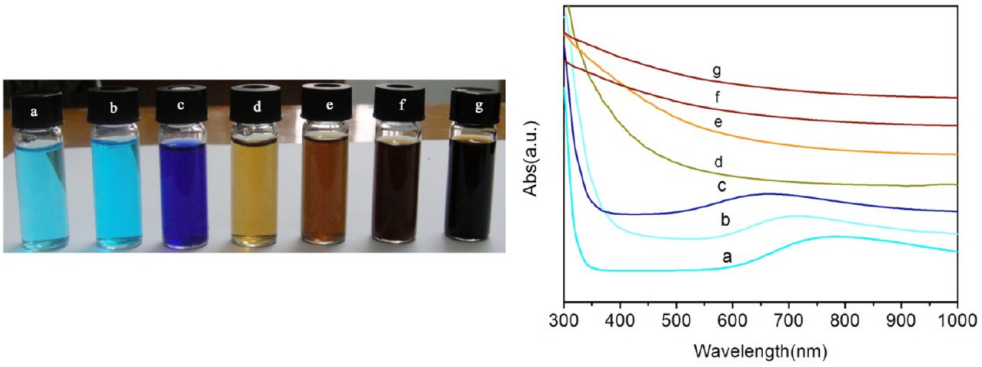

Figure 1. Photographs and the UV−vis absorption spectra as the color changed at different reaction periods: (a) copper acetate solution, (b) addition of lactic acid, (c) addition of ammonia−water, and after addition of hydrazine hydrate: (d) 2 min, (e) 10 min, (f) 30 min, (g) 60 min.

capped by PVP at 150 °C decreased to 24 $\mu\Omega$·cm because of the effect of the particle size on the recrystallization of the strained metal nanoparticles. However, PVP does not decompose at this temperature and remains as a shell on the surface of the copper nanoparticles.[18] Researchers have reported that oleic acid and lauric acid can both act as a particle protector on account of their carboxyl end groups coordinating to the surface of the newly generated copper nanoparticles, thereby playing an important role in preventing the copper particles from undergoing oxidation.[19−21] However, organic solvents, such as acetone and toluene, have to be used because of the low solubility of oleic acid and lauric acid in water. Dieste et al. reported that oleic acid-protected Co and Ni nanocrystals showed complete thermal desorption at ca. 200 °C and dehydrogenation at ca. 400 °C, leaving a graphitic surface with alkane fragments underneath.[22] Xiong et al. synthesized copper nanoparticles in aqueous medium by means of utilizing L-ascorbic acid as both reducing agent and capping agent, which prevented the generated copper nanoparticles from undergoing oxidation and aggregation.[23] However, the sintering of such copper nanoparticles was not reported by Xiong et al. It is widely understood that sintering of copper particles takes place at high temperatures when all the organic material has been burnt off and necks begin to form between the remaining particles. The lowest temperature at which printed features become conductive is mainly determined by the organic capping agent in the ink.[24−27] We believe that L-ascorbic acid-stabilized copper nanoparticles are not easily sintered at low temperature because of the relatively high decomposition temperature of L-ascorbic acid (221 °C).[28]

We recently reported that lactic acid-stabilized copper nanoparticles are antioxidative and can be easily sintered at low temperature.[29] In this paper, we report a simple and high-throughput method for the preparation of copper nanoparticles in aqueous solution. The desirable antioxidation property and the low decomposition temperature of short chain carboxylic acids are applied in the synthesis and sintering of copper nanoparticles.

2. EXPERIMENTAL SECTION

Materials. Copper(II) acetate monohydrate, hydrazine hydrate solution (50%), lactic acid, glycolic acid, acetic acid, citric acid, glycine, alanine, and ammonia−water were purchased from Sinopharma Chemical Reagent Co., Ltd. All chemicals were used as received without further purification.

Characterization. The sizes and distributions of copper nanoparticles were analyzed using a Hitachi H600 transmission electron microscope (TEM). UV−vis absorption spectra were recorded on a Hitachi U-4100 spectrophotometer. Crystal structures were determined by X-ray diffraction (XRD) using a Rigaku D/max-rB advanced X-ray diffractometer with CuKα radiation. Fourier transform infrared (FT-IR) spectra were recorded on a Nicolet Nexus 470 FT-IR spectrophotometer operating at a resolution of 4 cm^{-1}. X-ray photoelectron spectroscopy (XPS) spectra were recorded on a Kratos Axis Ultra DLD photoelectron spectrometer using an AlKα X-ray excitation source. Thermogravimetric analysis (TGA) was carried out using a Shimazu DTG-60H thermal gravimetric analyzer with a heating rate of 10 °C min^{-1} under nitrogen. The microstructure of the sintered copper film was analyzed using a field emission scanning electron microscope (JEOL, JEM-6701F). The thickness of the film was measured using a surface profiler (Tencor Instruments, Alpha-Step 200). The resistivity of the copper film was measured using a Shanghai Qianfeng SB100A/2 four-point probe meter and calculated according to the literature.[30]

Synthesis of Copper Nanoparticles. Copper nanoparticles were synthesized by chemical reduction of copper ions in aqueous solution at room temperature in air. In a typical procedure, 0.05 mol of copper acetate monohydrate was dissolved in 50 mL of water, and 0.70 mol of carboxylic acid was injected under constant stirring with a magnetic stirrer. Ammonia−water was added to the solution until the pH reached 10. Then, 0.1 mol of hydrazine hydrate was added, and the mixture was stirred vigorously for 1 h. The conversion of the copper salt to copper nanoparticles was monitored by the color change over different reaction periods. Along with the progression of the reaction, the color changed from light blue to deep blue, yellow, then brown, and finally henna. The solution was centrifuged at 11 000 rpm for 15 min. A small amount of henna-colored copper nanoparticles precipitated at the bottom of the centrifuge tube, which was easily dispersed in the solution again upon slight shaking. To obtain a sufficient quantity of copper nanoparticles, the solution was aged at 40 °C for 3 h in an inert atmosphere. The settled henna-colored copper nanoparticles were washed with ethanol to remove any unreacted reactants, and then dried in vacuum.

Preparation of Copper Films. The copper nanoparticles synthesized above were redispersed in ethanol forming a paste with a concentration of 10 wt %. Copper films were prepared by depositing the paste onto glass slides and drying the coated slides under vacuum for 1 h. The copper film thickness was controlled by depositing a fixed amount of the copper paste onto the glass slide within a fixed area. The copper films were annealed at 100, 150, 200, and 250 °C for 60 min under nitrogen. The thickness of the sintered film was 9.2 ± 1.5 μm.

3. RESULTS AND DISCUSSION

3.1. Preparation and Characterization of Copper Nanoparticles. Copper nanoparticles were synthesized by reduction of copper acetate with hydrazine using functionalized short chain carboxylic acids as capping agents. The process was

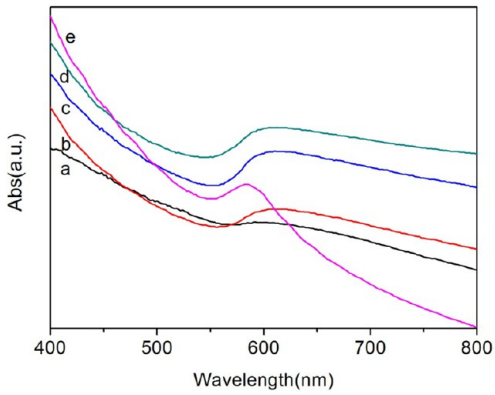

Figure 2. UV−vis absorption spectra of dispersed copper nanoparticles synthesized using different carboxylic acids as capping agents: (a) acetic acid, (b) glycolic acid, (c) alanine, (d) lactic acid, and (e) citric acid.

conducted on a large scale (1.0 mol/L) in aqueous solution at room temperature in a short time. The reaction mixture changed with the progression of the reaction, from light blue to deep blue, yellow then brown, and finally henna. To follow the reaction process, the color change of the reaction mixture was monitored by taking photographs and UV−vis absorption spectra at different reaction periods, as shown in Figure 1. Samples of the solution were taken at seven typical phases: initial copper acetate solution, after addition of lactic acid, after addition of ammonia−water, and 2, 10, 30, and 60 min after addition of hydrazine hydrate. As the lactic acid and ammonia−water were added, the Cu^{2+} peak at about 800 nm shifted to a shorter wavelength in the UV−vis absorption spectra. After the addition of the hydrazine hydrate, the Cu^{2+} peak disappeared and no new characteristic peak related to copper nanoparticles appeared as the reaction progressed, even when the solution turned henna color. After addition of hydrazine hydrate for 30 and 60 min, the color of the solution and the UV−vis absorption spectra did not change any more.

The absorption bands of copper nanoparticles are in the range 550−600 nm.[20] The surface plasmon resonance phenomena of copper nanoparticles could not be detected from the original reaction mixture, probably due to the nanoparticles being coated by a large amount of lactic acid in the solution. After the synthesized nanoparticles were separated, washed, and redispersed in ethanol, the copper nanoparticles exhibited surface plasmon resonance characteristics. Figure 2d shows the UV−vis absorption spectrum of the redispersed copper nanoparticles. The absorption peak for the copper nanoparticles occurs at 600 nm. We believe that the color changes are related to the reaction that takes place in solution: copper ions are first coordinated with lactic acid and ammonia, which are then reduced to zerovalent copper.[31] However, a more detailed analysis is needed to illustrate the mechanism of reaction.

The pH of the reaction medium, which is adjusted by the addition of ammonia−water, plays an important role in the synthesis of copper nanoparticles. Copper films were immediately generated on the wall of the flask following the addition of hydrazine hydrate if the pH was less than 10. It has been reported that the pH affects the progress of copper reduction in aqueous media.[32,33] At too low a pH, a rapid release of hydrogen bubbles produces a large amount of Cu nuclei, which aggregate into large agglomerates. Gorup et al. reported that silver(I) diammonia complexes play an important role in the synthesis and stabilization of small sized metallic silver nanoparticles.[34] We think that the formation of copper(II)−ammonia complexes plays a similar role by decreasing the reduction rate and thus stabilizing the growth of copper nanoparticles.

The concentration of lactic acid influences the size and uniformity of the copper nanoparticles. Figure 3 shows TEM images of the copper nanoparticles formed using different concentrations of lactic acid as capping agent. As the concentration of lactic acid increases, the size of the copper nanoparticles gradually decreases and becomes more uniform. When the concentration of lactic acid is 14.0 mol/L, the size of the copper nanoparticles is less than 10 nm. When the concentration of lactic acid is 2.8 mol/L, the copper film takes 3 h to deposit on the wall of the flask. The deposition rate of the copper film also depends on the concentration of lactic acid. The deposition rate decreases with increasing lactic acid concentration. When the concentration of lactic acid increases to 14.0 mol/L, no copper film is deposited on the wall of the flask, even after 1 month of storage.

It is believed that the size of the copper nanoparticles can be effectively controlled by changing the concentration of the capping agent. The growth of the copper nanoparticles is influenced by the strength of adsorption of the encapsulating ligands and the competition between the interparticle aggregation for the growth of particles and the molecular encapsulation for the stabilization of the nanoparticles.[21] Schadt et al. have demonstrated that monolayer-protected gold nanoparticles can be tuned by manipulating the concentration and the chain length of alkanethiols in the processing

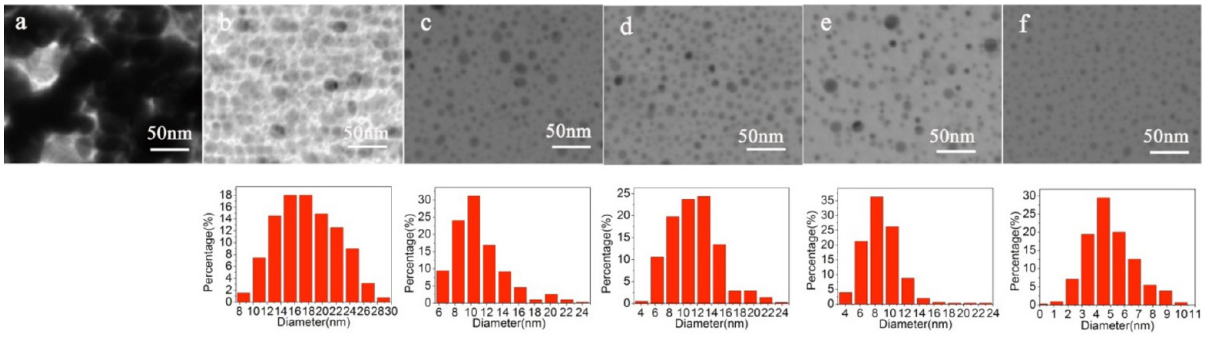

Figure 3. TEM images and particle size distribution of copper nanoparticles stabilized with lactic acid in different concentrations: (a) 0 mol/L, (b) 2.8 mol/L, (c) 5.6 mol/L, (d) 8.4 mol/L, (e) 11.2 mol/L, and (f) 14 mol/L.

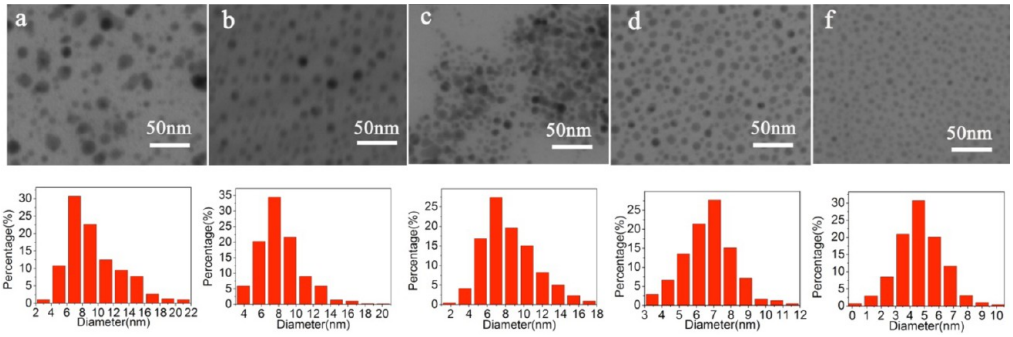

Figure 4. TEM images and particle size distribution of copper nanoparticles synthesized using different carboxylic acids as capping agents (14 mol/L): (a) acetic acid, (b) glycolic acid, (c) glycine, (d) alanine, and (e) citric acid.

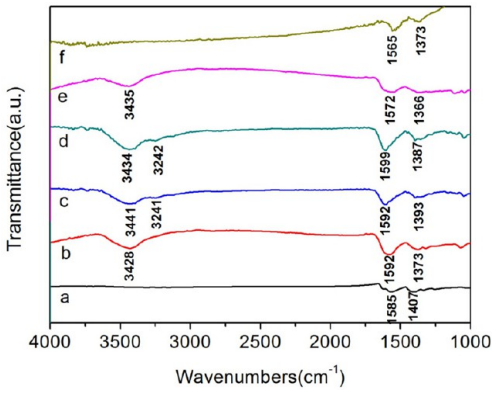

Figure 5. FT-IR spectra of copper nanoparticles synthesized using different carboxylic acids as capping agents: (a) acetic acid, (b) glycolic acid, (c) glycine, (d) alanine, (e) lactic acid, and (f) citric acid.

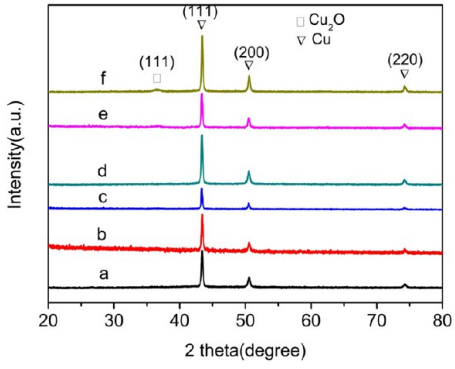

Figure 6. XRD patterns of copper nanoparticles synthesized using different carboxylic acids as capping agents: (a) acetic acid, (b) glycolic acid, (c) glycine, (d) alanine, (e) lactic acid, and (f) citric acid.

solution.[35] The change in alkanethiol concentration shifts the evolution equilibrium in terms of shell desorption and re-encapsulation, and the increase in alkanethiol chain length leads to a gain in stabilization energy due to additional interchain cohesive interactions.

Compared with the commonly used capping agents containing long alkyl chains, the short chain carboxylic acids have the advantage of low decomposition temperature, antioxidation, and reductive capability. To further confirm the use of short chain carboxylic acids as capping agents to synthesize copper nanoparticles with controlled size, acetic acid, glycolic acid, glycine, alanine, and citric acid were used. When the concentration of these capping agents was 2.8 mol/L, the copper film appeared on the wall of the flask in about 3 h. When the concentration of these capping agents increased to 14.0 mol/L, no copper nanoparticles precipitated from solution. This trend is similar to that observed with lactic acid.

Figure 4 shows TEM images of copper nanoparticles synthesized using acetic acid, glycolic acid, glycine, alanine, and citric acid as capping agents (14 mol/L). The size and dispersibility of the copper nanoparticles increases in the order of citric acid, lactic acid, alanine, glycolic acid, glycine, and acetic acid. The particle sizes and particle distributions are comparable for citric acid and lactic acid capped copper nanoparticles, as shown in Figure 4e and Figure 3f. The alanine capped copper nanoparticles are slightly larger when compared to the citric acid and lactic acid capped particles, as shown in Figure 4d. The size of the particles is larger when acetic acid, glycolic acid, or glycine are used as capping agents. In the case of glycine, the particles agglomerate (Figure 4c). It is clear that the size, distribution, and dispersibility of the copper nanoparticles are influenced by the chain length and the functional group of the acids. For smaller particle size and better dispersibility of the copper nanoparticles, a carboxylic capping agent with at least three carbons is preferred. The greater the number of functional groups on the capping agent, the smaller the size and better dispersibility of the nanoparticles. These can be explained by the cohesive interactions in regulating the interfacial reactivity of the preformed nanoparticles. The longer the chain length of the capping agent, the larger the cohesive energy resulting from the van der Waals interaction. The difference in the cohesive energy thus regulates the degree of coalescence and re-encapsulation and ultimately results in the size difference of the particles.[35]

Similarly, the surface plasmon resonance of the copper nanoparticles using other carboxylic acids as capping agents could not be detected in the original reaction mixture. After the synthesized nanoparticles were separated, washed, and redispersed in ethanol, the UV−vis spectra of the dispersed copper nanoparticles with acetic acid, glycolic acid, alanine, lactic acid, or citric acid were obtained (Figure 2). Because of the fast sedimentation, the UV−vis spectrum of the copper nanoparticles synthesized with glycine as the capping agent could not be measured. The UV−vis absorption peaks for copper nanoparticles prepared with acetic acid, glycolic acid, alanine, lactic acid, and citric acid occur at 616, 610, 601, 600, and 582 nm, respectively. The changes in peak wavelength are in accordance with the size of the nanoparticles observed in the TEM images, indicating that the redispersibility of the copper nanoparticles is influenced by the carbon chain length and the functional groups of the carboxylic acid. Citric acid with the

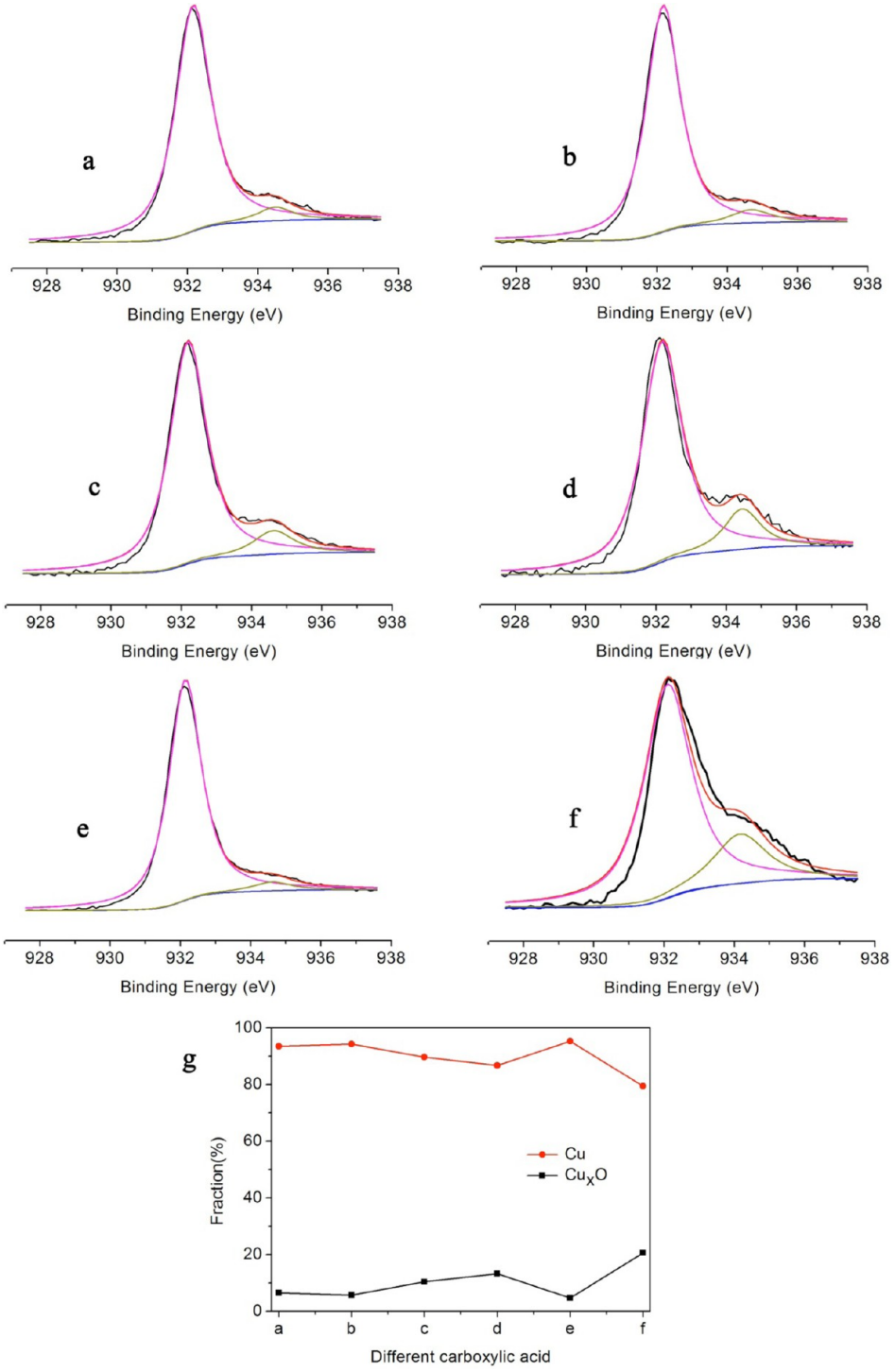

Figure 7. Peak fitting of the Cu2p3/2 spectra of copper nanoparticles synthesized using different carboxylic acids as capping agents: (a) acetic acid, (b) glycolic acid, (c) glycine, (d) alanine, (e) lactic acid, and (f) citric acid. (g) XPS based semiquantitative analysis.

longer carbon chain shows an obvious advantage in the redispersibility of copper nanoparticles.

The FT-IR spectra of the ethanol-washed copper nanoparticles synthesized using different carboxylic acids as capping agents are shown in Figure 5. The peaks at 1608−1561 and 1395−1375 cm^{-1} are attributed to the asymmetric and symmetric stretching of the conjugate carboxylates, respectively. The amine peaks of the copper nanoparticles capped by glycine and alanine occur around 3400−3200 cm^{-1} (Figure 5c and d). The strong absorption at 3400 cm^{-1} is probably from the adsorbed water. The peaks around 3400 cm^{-1} in Figure 5b and e are attributed to the hydroxyl groups of glycolic acid and lactic acid, respectively. It is clear that the carboxylates are adsorbed on the surface of the copper nanoparticles after most of the capping agents are washed off by ethanol.

Figure 6 shows the XRD patterns of the ethanol-washed copper nanoparticles, synthesized with different carboxylic acids as capping agents. In the case of acetic acid, glycolic acid, glycine, alanine, and lactic acid, the XRD pattern shows three characteristic peaks at 43.2°, 50.3°, and 74.1° for the marked

dx.doi.org/10.1021/am400480k | ACS Appl. Mater. Interfaces 2013, 5, 3839−3846

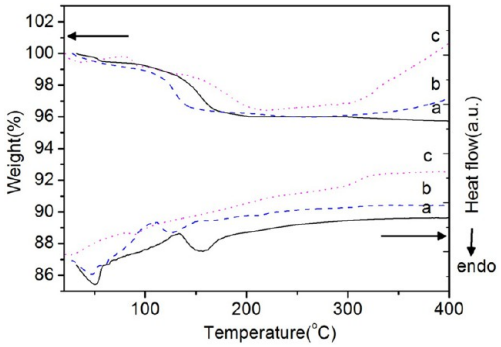

Figure 8. TGA of the copper film formed using different capping agents before sintering: (a) lactic acid, (b) glycolic acid, and (c) acetic acid.

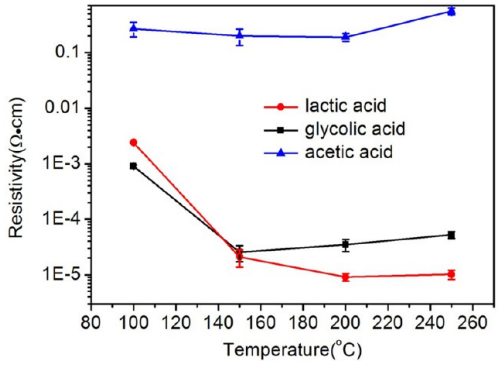

Figure 9. Resistivity of the films formed using different capping agents sintered at different temperatures under nitrogen.

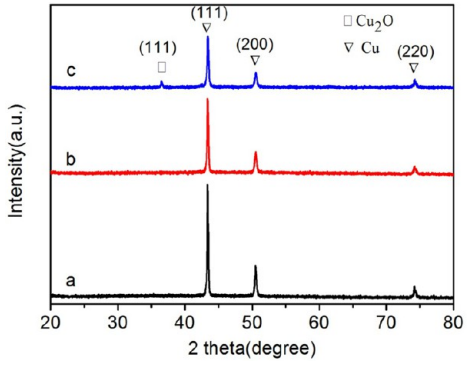

Figure 10. XRD pattern of the copper films formed using different capping agents after sintering at 200 °C: (a) lactic acid, (b) glycolic acid, and (c) acetic acid.

indices of (111), (200), and (220), respectively. These characteristic peaks confirm the formation of a face-centered cubic (FCC) copper phase without significant oxides or other impurity phases. When citric acid was used as the capping agent, the minor Cu_2O phase was detected at 36.6° in addition to the main phase of copper.

Because the surface oxide layer is amorphous and small in volume, XRD may not be suitable for analyzing the trace surface oxide. To probe the extent of surface oxidation of copper nanoparticles, XPS analysis was performed. Figure 7 shows the peak fitting of the Cu2p3/2 spectra of copper nanoparticles with different carboxylic acids as capping agents. The peaks at 932.1 and 934.6 eV are attributed to Cu and CuO, respectively.[36,37] Based on the semiquantitative analysis, the atomic fraction of the surface oxide layer of copper nanoparticles is influenced by the capping agent. When acetic acid, glycolic acid, and lactic acid are used as capping agents, the surface oxide layer on the copper nanoparticles is less than 7% because the longer chain lengths and additional hydroxyl groups are densely packed on the copper surface. The copper nanoparticles synthesized using lactic acid as the capping agent had the lowest surface oxide. The densely packed layer of adsorbed capping agent on the Cu surface blocks oxygen atoms to the metal during particle synthesis, resulting in reduced surface oxidation and thus a thinner oxide layer.[36] The atomic faction of the surface oxide layer is more than 10% when glycine and alanine are used as capping agents. In the case of citric acid, the atomic fraction of the surface oxide layer reached 20%. It is possible that the formation of the strong chelate complex of glycine, alanine, and citric acid with cupric salt decreases the rate of reduction. Thus, a minor cuprous compound, which has not been completely reduced, may adhere on the surface of the copper nanoparticles forming cuprous oxide. Cu_2O is not stable in air and easily oxidizes to CuO on the surface. Therefore, the XRD and XPS results of the copper nanoparticles using citric acid as capping agent show a copper oxide phase.

3.2. Characterization of Copper Films. Figure 8 shows the thermogravimetric analysis (TGA) and differential thermal analysis curves (DTA) of copper films formed using lactic acid, glycolic acid, and acetic acid as capping agents under a nitrogen atmosphere. An endothermic peak observed in the DTA curves at 50 °C is attributed to the evaporation of residual solvent corresponding to a weight loss of less than 0.5%. Another endothermic peak, related to a weight loss of 4%, is observed at about 156 and 125 °C for the lactic acid and glycolic acid capped copper films, respectively. For the acetic acid capped copper film, the endothermic peak at 91 °C is very weak and the corresponding weight loss is only about 1%. The complete decomposition finishes at about 200 °C with a weight loss of 4%. Thus, the capped acetic acid is hardly decomposed around the endothermic peak compared with the other two capping agents. It is noted that the weight gain after 300 °C was observed in the TGA curve of the acetic acid capped copper film, which is due to the oxidation of copper.

Mott et al. confirmed that the melting point of 6-nm-diameter copper nanoparticles began at around 450 °C with a maximum near 550 °C. However, the size dependence of the melting temperature of the copper nanoparticles, especially for surface melting, plays an important role in interparticle coalescence.[21] As the temperature increases, the desorption of the capping agent from the nanoparticle surface is favored, thereby increasing the opportunities for interparticle coalescence. Based on the TGA and DTA results using lactic acid, glycolic acid, and acetic acid as capping agents, we believe most of the carboxylates adsorbed on the copper nanoparticle's surface can be removed at a relatively low temperature, which may facilitate the interparticle coalescence.

The electrical resistivity of the films was measured using a four-point probe technique. Before sintering all films were nonconducting. The resistivity of the film using lactic acid as capping agent is 21.0 ± 7.0 and 9.1 ± 2.0 $\mu\Omega$·cm after sintering at 150 and 200 °C for 60 min under nitrogen, respectively (Figure 9). The latter reaches about 19% of the conductivity of bulk copper, and is comparable with previously reported values of 11[36,37] and 17 $\mu\Omega$·cm.[38] The resistivity of the film sintered at higher temperature (250 °C) increases slightly. The resistivity

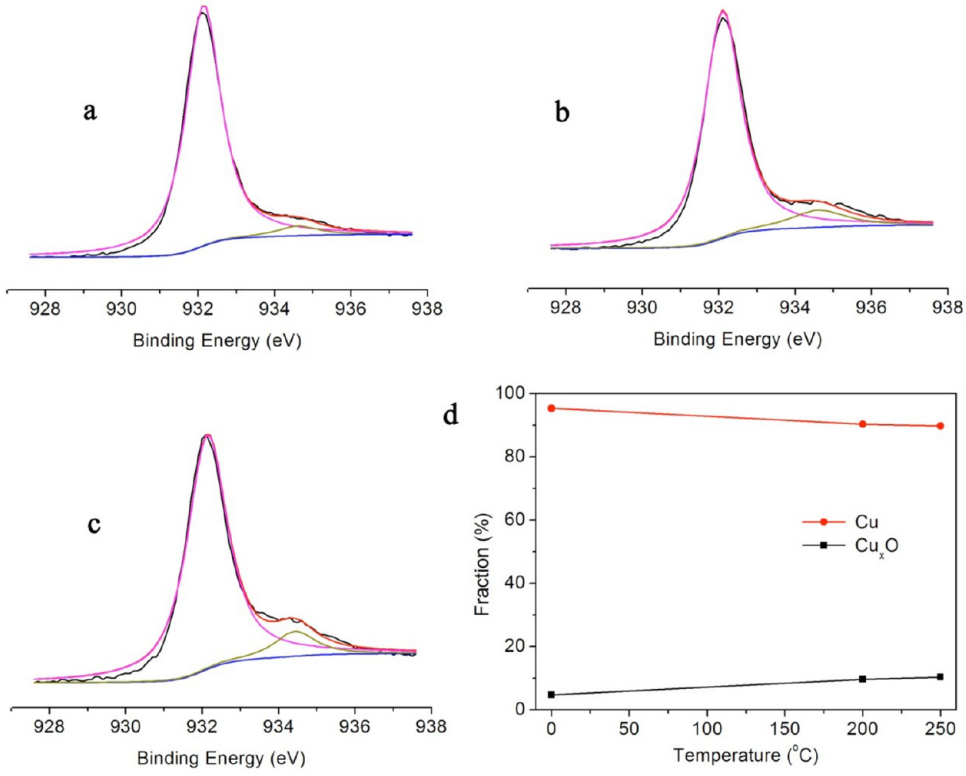

Figure 11. Peak fitting of the Cu2p3/2 spectra of copper film formed using lactic acid as capping agent sintered at different temperatures under nitrogen: (a) before sintering, (b) 200 °C, and (c) 250 °C; and (d) XPS based semiquantitative analysis.

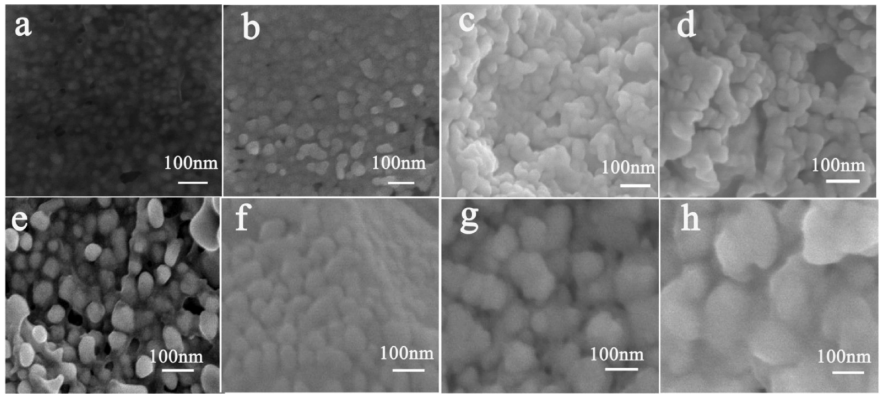

Figure 12. SEM images of microstructure of the films annealed at different temperatures. Lactic acid as the capping agent: (a) 100, (b) 150, (c) 200, and (d) 250 °C; glycolic acid as the capping agent: (e)100, (f) 150, (g) 200, (h) 250 °C.

of the film using glycolic acid as capping agent is 25.5 ± 8.0 and 34.8 ± 8.0 $\mu\Omega$·cm after sintering at 150 and 200 °C, respectively. The resistivity of the film increases slightly as the sintering temperature increases. In the case of using acetic acid as capping agent, the resistivity of the film is poor after sintering at different temperatures. The high resistivity is probably due to the difficult decomposition of the capping agent and the oxidation of the copper film as observed in the TGA curve.

Figure 10 shows XRD patterns of these films after sintering at 200 °C under nitrogen. The XRD pattern of the copper films formed using lactic acid and glycolic acid as capping agents show three characteristic peaks at 43.2°, 50.3°, and 74.1° for the marked indices of (111), (200), and (220), respectively. These characteristic peaks confirm that the copper films are not oxidized after sintering. However, using acetic acid as a capping agent, a tiny peak indexed as the (111) diffraction of Cu_2O appeared, which is associated with the oxidation of the metallic copper. We believe that lactic acid and glycolic acid, with an additional hydroxyl functional group, can better protect the copper from oxidation.

The XPS study was performed to elaborate the oxidation state of the sintered copper film. Figure 11 shows the peak fitting of the Cu2p3/2 spectra of the copper films using lactic acid as capping agent before and after sintering. After sintering at 200 °C, the fraction of the oxide layer increases from 5% to 10% (Figure 10d), which confirms the formation of an additional oxide after the capping agent decomposition. As the sintering temperature increases to 250 °C, the oxide content on the surface increases slightly.

SEM images of the microstructure of the copper films formed using lactic acid and glycolic acid as capping agents after

dx.doi.org/10.1021/am400480k | ACS Appl. Mater. Interfaces 2013, 5, 3839−3846

sintering from 100 to 250 °C are shown in Figure 12. The microstructure of the films shows the trend of interparticle coalescence as the sintering temperature increased. It can be seen that most nanoparticles are still isolated after sintering at 100 °C. However, as the sintering temperature increases to 150 °C, the removal of the previously adsorbed carboxylate groups allows the fresh copper nanoparticle surface to coalesce and form a continuous layer. When the sintering temperature reaches 200 °C, most of the nanoparticles have fused together to form a network throughout the entire copper film.

CONCLUSIONS

The present study illustrates a high-throughput, simple, and convenient method for the synthesis of copper nanoparticles through the reduction of copper salts in aqueous medium. We have successfully demonstrated that short chain carboxylic acids can be used as capping agents to obtain copper nanoparticles. When citric acid, alanine, or lactic acid are used in high concentrations stable copper nanoparticles with a narrow size distribution and an average diameter of less than 10 nm are obtained. When glycolic acid is used as the capping agent, highly conductive copper films with electrical resistivity of 25.5 ± 8.0 and 34.8 ± 9.0 $\mu\Omega$·cm after annealing at 150 and 200 °C for 60 min under nitrogen, respectively, are obtained. When lactic acid is used as the capping agent, the electrical resistivity of the copper films is 21.0 ± 7.0 and 9.1 ± 2.0 $\mu\Omega$·cm after annealing at 150 and 200 °C for 60 min under nitrogen, respectively. We believe that the simple synthesis of copper nanoparticles with low sintering temperature allows the fabrication of printed copper patterns on plastic substrates.

AUTHOR INFORMATION

Corresponding Author

*E-mail: feixiao@fudan.edu.cn. Fax: +86-21-65103056. Tel: +86-21-65642110.

Notes

The authors declare no competing financial interest.

ACKNOWLEDGMENTS

This study was supported by National Science and Technology Major Project with contracts 2009ZX02038 and 2011ZX02602.

REFERENCES

(1) Li, Y.; Wong, C. P.; Lu, D. In *Electrical Conductive Adhesives with Nanotechnologies*, 1st ed.; Springer: New York, 2010; p 303.
(2) Li, D. P.; Sutton, D.; Burgess, A.; Graham, D.; Calvert, P. D. *J. Mater. Chem.* **2009**, *19*, 3719−3724.
(3) Ko, S. H.; Pan, H.; Grigoropoulos, C. P.; Luscombe, C. K.; Fréchet, J. M. J.; Poulikakos, D. *Nanotechnology* **2007**, *18* (345202), 1−8.
(4) Hon, K. K. B.; Li, L.; Hutchings, I. M. *CIRP Ann.* **2008**, *57*, 601−620.
(5) Schmid, G.; Corain, B. *Eur. J. Inorg. Chem.* **2003**, *17*, 3081−3098.
(6) Volker, E.; Benaskar, F.; Jefferson, D. A.; Johnsona, B. F. G.; Wheatley, A. E. H. *Dalton Trans.* **2010**, *39*, 6496−6502.
(7) Jeong, S.; Song, H. C.; Lee, W. W.; Choi, Y. M.; Lee, S. S.; Ryu, B. H. *J. Phys. Chem. C* **2010**, *114*, 22277−22283.
(8) Walker, S. B.; Lewis, J. A. *J. Am. Chem. Soc.* **2012**, *134*, 1419−1421.
(9) Smith, P. J.; Shin, D. Y.; Stringer, J. E.; Derby, B. *J. Mater. Sci.* **2006**, *41*, 4153−4158.
(10) Lee, K. J.; Jun, B. H.; Kim, T. H.; Joung, J. *Nanotechnology* **2006**, *17*, 2424−2428.
(11) Lin, J. C.; Chan, J. Y. *Mater. Chem. Phys.* **1996**, *43*, 256−265.
(12) Chen, S. W.; Sommers, J. M. *J. Phys. Chem. B* **2001**, *105*, 8816−8820.
(13) Foresti, E.; Fracasso, G.; Lanzi, M.; Lesci, I. G.; Paganin, L.; Zuccheri, T.; Roveri, N. *J Nanomater.* **2008**, *649130*, 1−6.
(14) Yang, J. G.; Zhou, Y. L.; Okamoto, T.; Bessho, T.; Satake, S.; Ichino, R.; Okido, M. *Chem. Lett.* **2006**, *35*, 1190−1191.
(15) Huaman, J. L. C.; Sato, K.; Kurita, S.; Matsumotoc, T.; Jeyadevan, B. *J. Mater. Chem.* **2011**, *21*, 7062−7069.
(16) Magdassi, S.; Grouchko, M.; Kamyshny, A. *Materials* **2010**, *3*, 4626−4638.
(17) Folarin, O. M.; Sadiku, E. R.; Maity, A. *Int. J. Phys. Sci.* **2011**, *6*, 4869−4882.
(18) Choi, C. S.; Jo, Y. H.; Kim, M. G.; Lee, H. M. *Nanotechnology* **2012**, *23* (065601), 1−8.
(19) Jin, W. N.; Li, J.; Liu, S. J.; Chen, Q. Y. *Colloids Surf., A* **2011**, *373*, 29−35.
(20) Khanna, P. K.; Kale, T. S.; Shaikh, M.; Rao, N. K.; Satyanarayana, C. V. V *Mater. Chem. Phys.* **2008**, No. 110, 21−25.
(21) Mott, D.; Galkowski, J.; Wang, L.; Luo, J.; Zhong, C. J. *Langmuir* **2007**, *23*, 5740−5745.
(22) Dieste, V. P.; Castellini, O. M.; Crain, J. N.; Eriksson, M. A.; Kirakosian, A.; Lin, J. L.; McChesney, J. L.; Himpsel, F. J. *Appl. Phys. Lett.* **2003**, *83*, 5053−5055.
(23) Xiong, J.; Wang, Y.; Xue, Q. J.; Wu, X. D. *Green Chem.* **2011**, *13*, 900−904.
(24) Perelaer, J.; Schubert, U. S. In *Radio Frequency Identification Fundamentals and Applications Design Methods and Solutions*, 1st ed.; Turcu, C., Ed.; Intech: Rijeka, Croatia, 2010; p 265.
(25) Pulkkinen, P.; Shan, J.; Leppänen, K.; Känsäkoski, A.; Laiho, A.; Järn, M.; Tenhu, H. *ACS Appl. Mater. Interfaces* **2009**, *1*, 519−525.
(26) Ankireddy, K.; Vunnam, S.; Kellar, J.; Cross, W. *J. Mater. Chem. C* **2013**, *1*, 572−579.
(27) Jung, I.; Shin, K.; Kima, N. R.; Lee, H. M. *J. Mater. Chem. C* **2013**, *1*, 1855−1862.
(28) Tang, Y. B. *J. Wuxi Univ. Light Ind.* **2003**, *22*, 102−105.
(29) Deng, D.; Cheng, Y.; Jin, Y.; Qi, T.; Xiao, F. *J. Mater. Chem.* **2012**, *22*, 23989−23995.
(30) Smits, F. M. *Bell Syst. Tech. J.* **1958**, 711−718.
(31) Yamamoto, M.; Kashiwagi, Y.; Nakamoto, M. *Langmuir* **2006**, *22*, 8581−8586.
(32) Dang, T. M. D.; Le, T. T. T.; Blanc, E. F.; Dang, M. C. *Adv. Nat. Sci.: Nanosci. Nanotechnol.* **2011**, *2* (015009), 1−6.
(33) Zhang, H. X.; Siegert, U.; Liu, R.; Cai, W. B. *Nanoscale Res. Lett.* **2009**, *4*, 705−708.
(34) Gorup, L. F.; Longo, E.; Leite, E. R.; Camargo, E. R. *J. Colloid Interface Sci.* **2011**, *360*, 355−358.
(35) Schadt, M. J.; Cheung, W.; Luo, J.; Zhong, C. *J. Chem. Mater.* **2006**, *18*, 5147−5149.
(36) Jeong, S.; Woo, K.; Kim, D.; Lim, S.; Kim, J. S.; Shin, H.; Xia, Y.; Moon, J. *Adv. Funct. Mater.* **2008**, *18*, 679−686.
(37) Jeong, S.; Song, H. C.; Lee, W. W.; Lee, S. S.; Choi, Y.; Son, W.; Kim, E. D.; Paik, C. H.; Oh, S. H.; Ryu, B. H. *Langmuir* **2011**, *27*, 3144−3149.
(38) Woo, K.; Kim, D.; Kim, J. S.; Lim, S.; Moon, J. *Langmuir* **2009**, *25*, 429−433.